SUPPORTING INFORMATION
for

Probing the Stability of Metal-Organic Frameworks by Structure-Responsive Mass Spectrometry Imaging

Yue Lin[1,2], Ke Min[1], Wende Ma[1], Xuezhi Yang[2], Dawei Lu[1], Zhenyu Lin[3], Qian Liu*[,1,4,5], Guibin Jiang[1,5]

[1] State Key Laboratory of Environmental Chemistry and Ecotoxicology, Research Center for Eco-Environmental Sciences, Chinese Academy of Sciences, Beijing 100085, China

[2] School of Environment, Hangzhou Institute for Advanced Study, UCAS, Hangzhou 310024, China

[3] Ministry of Education Key Laboratory for Analytical Science of Food Safety and Biology, Fujian Provincial Key Laboratory of Analysis and Detection for Food Safety, College of Chemistry, Fuzhou University, Fuzhou, Fujian, 350116, China

[4] Institute of Environment and Health, Jianghan University, Wuhan 430056, China

[5] University of Chinese Academy of Sciences, Beijing 100190, China

* Corresponding Author: Prof. Qian Liu. Email: qianliu@rcees.ac.cn.

Contents： **page**

1. Experimental details

1.1 Reagents and chemicals

CuBTC (hydrothermal synthesis), MOF-74 and ZIF-8 (Zn) was purchased from XFNANO (Nanjing, China). $Cu(QC)_2$, SIFSIX-1-Cu, SIFSIX-2-Cu-i, SIFSIX-3-Cu, CPL-1, CPL-2, CPL-5, and MIL-101(Cr) were bought from CHEMSOON (Shanghai, China). $Cu(NO_3)_2$ and BTC were purchased from Aladdin (Shanghai, China). The newly purchased (i.e., newly synthesized by the manufacturer) products were applied for the degradation test. Ethanol was bought from Sinopharm (Beijing, China) and ultrapure water was obtained from ultrapure water purification system (Merck Millipore, Darmstadt, Germany). All reagents and solvents were of analytical grade or better.

1.2 Characterization of MOFs by SEM, FTIR, XRD, UV-Vis absorption spectra, UV-Vis diffuse reflection spectra, Raman, thermogravimetric (TG) test and BET.

Newly prepared and aged Cu-MOFs were placed on a silicon wafer followed by drying for scanning electron microscopy (SEM) measurement. The SEM images were obtained by using a Hitachi S-3000N SEM (Tokyo, Japan). Samples for X-ray diffraction (XRD) and Fourier transform infrared spectroscopy (FTIR) were prepared by drying newly prepared and aged CuBTC in a drying oven at 70 °C for 5 h. The FTIR analysis was carried out using a Nicolet iS10 FT-IR spectrometer (Wisconsinin, USA) working at the range of 400-2500 cm^{-1} with a resolution of 4 cm^{-1} for 32 times. XRD was carried out on a Bruker D8 Advance XRD system with a Nifiltered Cu-Kα ($\lambda = 1.5418$ Å) using a step scan mode (0.03° per step) within the range of $5^{o} < 2\theta < 45^{o}$. Ultraviolet-Visible (UV-Vis) absorption spectra of $Cu(NO_3)_2$, BTC and CuBTC (1 mg/mL) were recorded on Metash X-8 UV-Vis spectrophotometer (Shanghai, China) ranging from 200 to 1000 nm and the rest of the MOFs were ranging from 200 to 600 nm. UV-Vis diffuse reflection spectra of CuBTC (10 mg) was recorded by Shimadzu UV-3600 UV-Vis-NIR spectrophotometer ranging from 200 to 800 nm. 1 μL of the CuBTC were dropped on the ITO for naturally drying, Raman characterization of CuBTC samples was performed after LDI-MS testing by Thermo Fisher Scientific DXR Raman microscope (Waltham, Massachusetts) and excited with a 780 nm laser (24 mW). Brunauer–Emmett–Teller (BET) measurements of CuBTC were conducted on a Micromeritics 3-Flex gas sorption analyzer and a weighed amount of newly prepared and aged CuBTC (~ 50 mg) were prepared. Before the measurement, the samples were degassed at 50 °C for 12 h. The N_2 (77 K) isotherms were measured using a liquid nitrogen bath (77 K). TG tests were performed using samples recovered after N_2 adsorption tests. All samples were heated at a constant rate of 10 °C min^{-1} up to 900 °C on a NETZSCH STA 449F3 thermal gravimetric analyzer in N_2 atmosphere.

1.3 Stability tests of Cu-MOFs in water and air

For stability test in air, CuBTC (1.00 mg) was dispersed in ethanol (1.00 mL), and then the mixture was spread (1.00 μL) on ITO glass sheets followed by incubation in the glass box (1.00 × 1.00 × 1.00 m) with the moist air of 80% relative humidity (RH) controlled by a humidifier. The samples were taken out for the following LD-SRMS measurements at time intervals of 10 min, 30 min, 24 h, 168 h, 336 h, 504 h, and 720 h.

1.4 Spatial difference test of CuBTC stability in moist air.

The ITO glass was immersed in 4 mg/mL CuBTC (solvent: ethanol) for 1 h and then dried in the oven at 70 °C. A patterned shield was put on the top of ITO glass and then the whole device was incubated in the glass box (1.00 × 1.00 × 1.00 m) with the moist air with the moist air of 80% RH controlled by a humidifier. for 12 h.

1.5 Adsorption of CO_2 by CuBTC in moist air

CuBTC (10.0 mg) was dispersed in ethanol (1.00 mL), and then the mixture was spread (1.00 μL) on ITO glass sheets followed by incubation in a glass box. CO_2 was introduced into the glass box (1.00 × 1.00 × 1.00 m) for 5 min at a flow velocity of 1 L/min and the glass box was continually aerated with CO_2 at a flow velocity of 1 mL/min. The humidity was controlled at 80% RH and the samples were taken out for the following MS measurements at time intervals of 30 min, 1 h, 72 h, 336 h, 720 h, and 840 h.

1.6 Measurement of Cu in CuBTC by LA-ICP-MS

The imaging of Cu in CuBTC was achieved by LA-ICP-MS consisting of a SHIMADZU 2030 ICP-MS coupled to a laser ablation (LA) system (NWR 213, Elemental Scientific Inc., NE, USA). LA was performed using a Nd:YAG laser with a wavelength of 213 nm and repetition frequency of 20 Hz in ablation mode of scanning line per line (spot size 50 μm, scan speed 100 μm/s, distance between lines 45 μm). The ablated samples were transported into the ICP-MS using He as carrier. It is noteworthy that only the CPS (count per second) of Cu was monitored in LA-ICP-MS imaging.

1.7 LDI-SRMS detection and imaging of Cu-MOFs

The LDI-SRMS analysis of all CuBTC (samples) was proceeded on a Bruker rapifleX matrix-assisted laser desorption ionization (MALDI) Tissuetyper (Bruker Daltonics) controlled by FlexControl software in the reflection and negative-ion mode. A 355 nm Nd:YAG laser with a frequency of 400 Hz and laser power of 40% was used. The spectra were recorded by summing 400 laser shots, and the FlexAnalysis 3.4 software was applied for data processing.

LDI-SRMS imaging of Cu-MOFs was performed on a rapifleX MALDI Tissuetyper controlled by FlexImaging and FlexControl software. All test samples were dried in a drying oven at 70 °C for 30 min before imaging analysis. The experiments of CuBTC samples were performed in the reflection and the negative-ion mode over a mass range of *m/z* 0-500 and other types of Cu-MOFs (Cu(QC)$_2$, SIFSIX-1-Cu, SIFSIX-2-Cu-i, SIFSIX-3-Cu, CPL-1, CPL-2 and CPL-5) were performed in the linear and the negative-ion mode over a mass range of *m/z* 2-800. The laser power was 80%, the laser pulse frequency was 400 Hz, the spatial resolution was 50 × 50 μm, and 400 shots were summed per array position. The calibration curves of CuBTC were built based on the average intensity of [BTC-COOH]$^-$ (*m/z* 165) outputted from imaging MS.

1.8 LDI-SRMS test of Cu(NO$_3$)$_2$ and BTC

Cu(NO$_3$)$_2$ (1.00 mg) and BTC (1.00 mg) were dispersed in distilled water (1.00 mL), and then the mixture was spread (1.00 μL) on an indium tin oxide (ITO) glass for the following LDI-SRMS measurements. The test conditions were the same as that of CuBTC.

1.9 LDI-SRMS imaging of non-copper MOFs

MOF-74(Zn) (1.00 mg), ZIF-8(Zn) (1.00 mg), MIL-101(Cr) (1.00 mg), and Ni-containing MOF (1.00 mg) were dispersed respectively in distilled water (1.00 mL) and then the mixture was added (1.00 μL) onto ITO glass sheets for the following LDI-SRMS measurements.

LDI-SRMS imaging of non-copper MOFs was performed on a RapifleX MALDI Tissuetyper controlled by FlexImaging and FlexControl software. All test samples were dried in a drying oven at 70 °C for 30 min before imaging analysis. The experiments of ZIF-8 (Zn), MIL-101(Cr) and Ni-containing MOF samples were performed in the reflection and negative-ion mode over a mass range of *m/z* 2-300 and MOF-74(Zn) were performed in the reflection and positive-ion mode over a mass range of *m/z* 2-300. The laser power was 90%, the laser pulse frequency was 400 Hz, the spatial resolution was 50 × 50 μm, and 400 shots were summed per array position.

2. Supplementary results and discussion

2.1 Quantification of CuBTC

The characteristic fragment (*m/z* at 165) generated by the loss of a carboxyl group of BTC in negative-ion mode was steadily obtained with high signal intensity. So, it was chosen as a quantitative marker. A good linearity was obtained within the range from 0.05 to 1.00 mg/mL ($y = 9.57x + 2.57$, $R^2 = 0.950$). The limit of detection was 0.05 mg/mL (i.e., 50.0 ng in mass as the sample volume was ~1 μL; Figure S4).

2.2 Characterization of CuBTC in water

The structure of CuBTC in the aquatic environment after different periods of exposure time including 5, 15, 40, 60, 120, 150, 180, and 240 min was characterized by XRD, FTIR, BET and TG. The XRD results showed the major diffraction peaks at [2 0 0], [2 2 0], and [2 2 2] planes at exposure time of 120 min, which was in consistence with the CuBTC patterns in the previous literature.[1] At exposure time of 150 min, the diffraction peak at [220] plane began to change but the crystalline structure of CuBTC was still largely maintained. However, the crystallographic planes were totally different at 180 min. The peak intensity of [200] planes disappeared and [222] planes decreased sharply, indicating the complete degradation of CuBTC in water. The FTIR spectra of CuBTC showed some variations mainly at characteristic bands of carboxylic acids such as the bands at 1150–1280 cm^{-1} for C–O stretching and the band at 1705 cm^{-1} for C=O stretching[2] as the exposure time being prolonged (Figure S8 and Figure S9). The N_2 adsorption-desorption isotherm (Figure S10) revealed an overall weakening trend in total N_2 uptakes capacity of CuBTC with the increase of exposure time in water. Notably, the N_2 uptake capacity remained relatively unchanged for the first 40 minutes of exposure. However, a marked decline was observed between 40 and 60 min, followed by a gradual decrease after 120 min (Figure S10). The detailed data of BET surface area, pore volume and pore size were showed in Table S2, displaying trends consistent with the changes in N_2 uptake capacity. Finally, we processed the TG analysis of those CuBTC. As showed in Figure S11, the temperature with the maximum CuBTC mass change rate has little change with the extension of time within 240 min, indicating that TG analysis may not effectively characterize the stability changes of CuBTC under these conditions.

2.3 The universality of the LDI-SRMS imaging techniques

MOFs have different compositions, degradation pathways and products. For example, the {110} surface is more easily degraded than the {100} of ZIF-8 under mild acidic conditions.[3] SIFSIX-1 series may transform from 3D frameworks into 2D layered structures while maintaining Cu-ligand coordination bonds.[4] However, our proposed technique of structure-response mass spectrometry (SRMS) imaging is achieved based on the variations in LDI-MS signals caused by changes in the structure of MOFs. In fact, the variations in LDI-MS signals are only dependent on the intactness of the structure (and its associated laser energy absorption capability). So, the universality of the method was tested with Cu-MOFs as well as MOFs with other metal centers. In addition to the two types of MOFs discussed in the main text, the other six Cu-MOFs materials could also produce specific LDI-SRMS signals. The SIXSIF series were synthesized by Cu^{2+} and 1,2-bis(4-pyridyl)ethyne and the CPL series were synthesized by Cu^{2+} and 2,3-pyrazinedicarboxylic acid, 4,4'-vinylenedipyridine, 4,4'-bipyridine or pyrazine under the different conditions. The detailed MS data of characteristic peaks are showed in Figure S17, S18 and Table S5. The imaging results of SIFSIX-1-Cu, SIFSIX-2-Cu-i and SIFSIX-3-Cu showed obvious changes with the extension of exposure time in water, and most of the intensity ratio of characteristic peaks changed regularly, indicating that the stability of these MOFs would be easily destroyed by water. However, the SEM results of SIFSIX-1-Cu and SIFSIX-2-Cu-i did not provide discernible information regarding morphological changes under these conditions. Therefore, the SRMS method should be more sensitive than SEM. For CPL-1, CPL-2, and CPL-5, almost no color change could be observed according to imaging results and the intensity ratio of characteristic peaks also showed little change. Similarly, the SEM of CPL-1, CPL-2 and CPL-5 showed no morphological differences, either (Figure S19). Therefore, these Cu-MOFs should have better stability in water, which was also consistent with the material nature description provided by the manufacturer.

The application of SRMS technique has been extended to the characterization of various non-copper MOFs. Four types of MOFs, including MIL-101(Cr), Ni-containing MOFs, ZIF-8(Zn) and MOF-74(Zn), were found to be capable of generating signals in LDI-MS (Figure S20). MOF-74(Zn) exhibited prominent characteristic peaks at *m/z* 24.0, 39.5, 48.0, and 64.0 in LDI-MS. The change in the SRMS imaging results over a 3-day period was observed based on the decrease of $I_{m/z\ 24.0}/I_{m/z\ 39.5}$ ratio. ZIF-8(Zn) exhibited distinct characteristic peaks at *m/z* 26.0, 42.0, 60.0, 65.0, 81.0, and 131 in LDI-MS. The change of SRMS imaging results in 3 days was obtained based on the decrease $I_{m/z\ 60.0}/I_{m/z\ 65.0}$ ratio. Thus, the stability of MOF-74(Zn) and ZIF-8(Zn) exhibited slight changes over a 3-day period. MIL-101(Cr) and Ni-containing MOFs exhibited complex characteristic peaks in LDI-MS (Figure S20); however, the SRMS imaging results remained almost unchanged over a 3-day period, indicating their high stability due to compositional and structural differences of the materials. We also measured UV absorption spectra for all tested MOFs and observed that the majority of the materials exhibited significant absorption peaks between 300 and 400 nm. This property accounted for their ability to absorb the laser energy and generate signals in LDI-MS (Figure S21).

Certainly, considering the extensive variety of nanomaterials, degradation substrates, and degradation products, further research is essential to understand the response of SRMS to a broader range of materials and their degradation processes. Nonetheless, we remain optimistic about the ongoing advancement and potential applicability of this technology in the field.

3. Supporting Figures

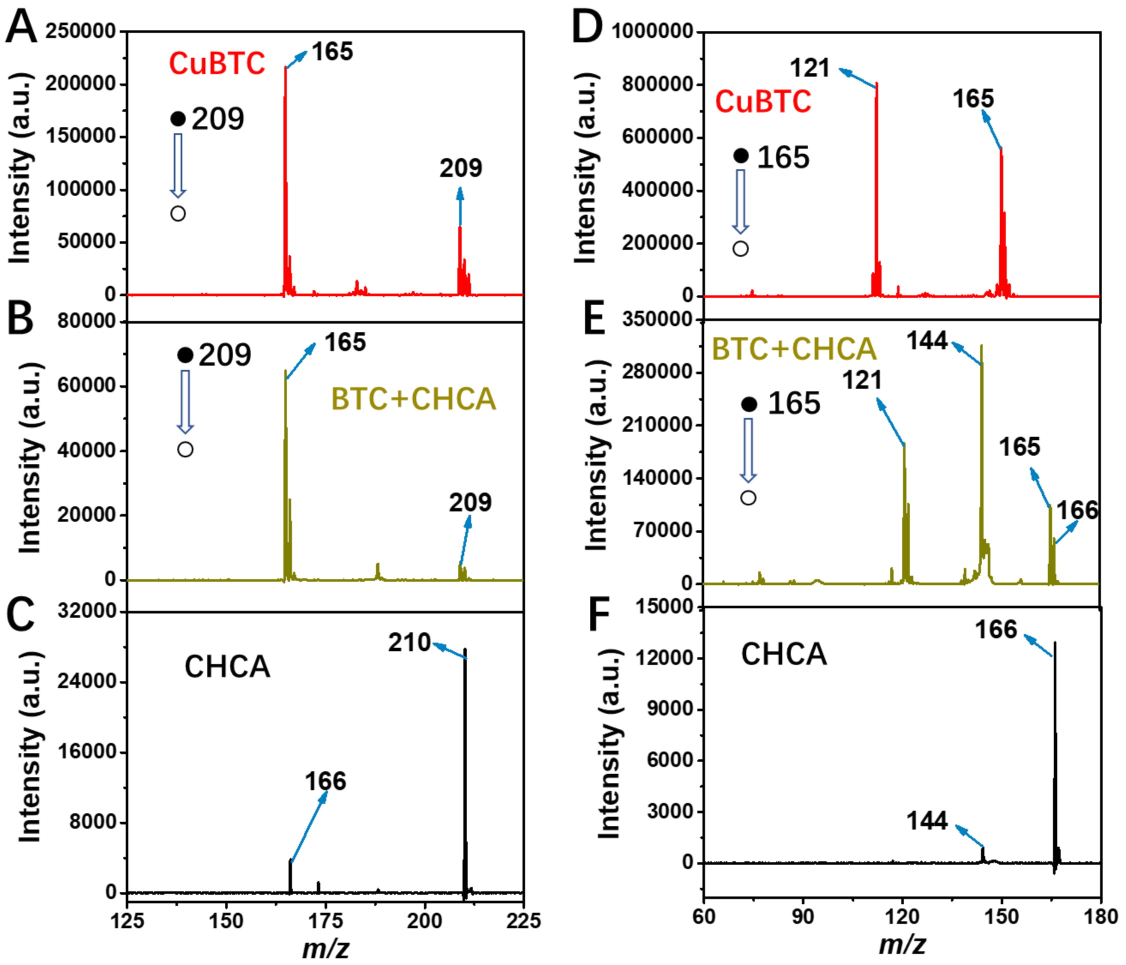

Figure S1. MS/MS spectra of precursor ion (*m/z* 209) obtained in MALDI-TOF MS/MS analysis of **(A)** CuBTC and **(B)** BTC+CHCA. **(C)** MS spectrum of CHCA in the *m/z* range of 125-225. MS/MS spectra of precursor ion (*m/z* 165) obtained from MALDI-TOF MS/MS analysis of **(D)** CuBTC and **(E)** BTC+CHCA. **(F)** MS spectrum of CHCA in the *m/z* range of 60-180.

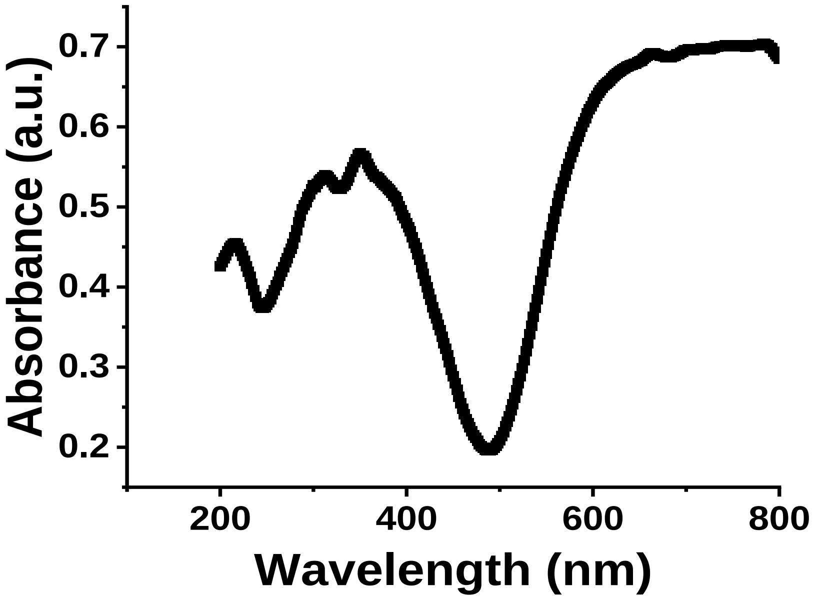

Figure S2. The UV-Vis diffuse reflection spectra of CuBTC.

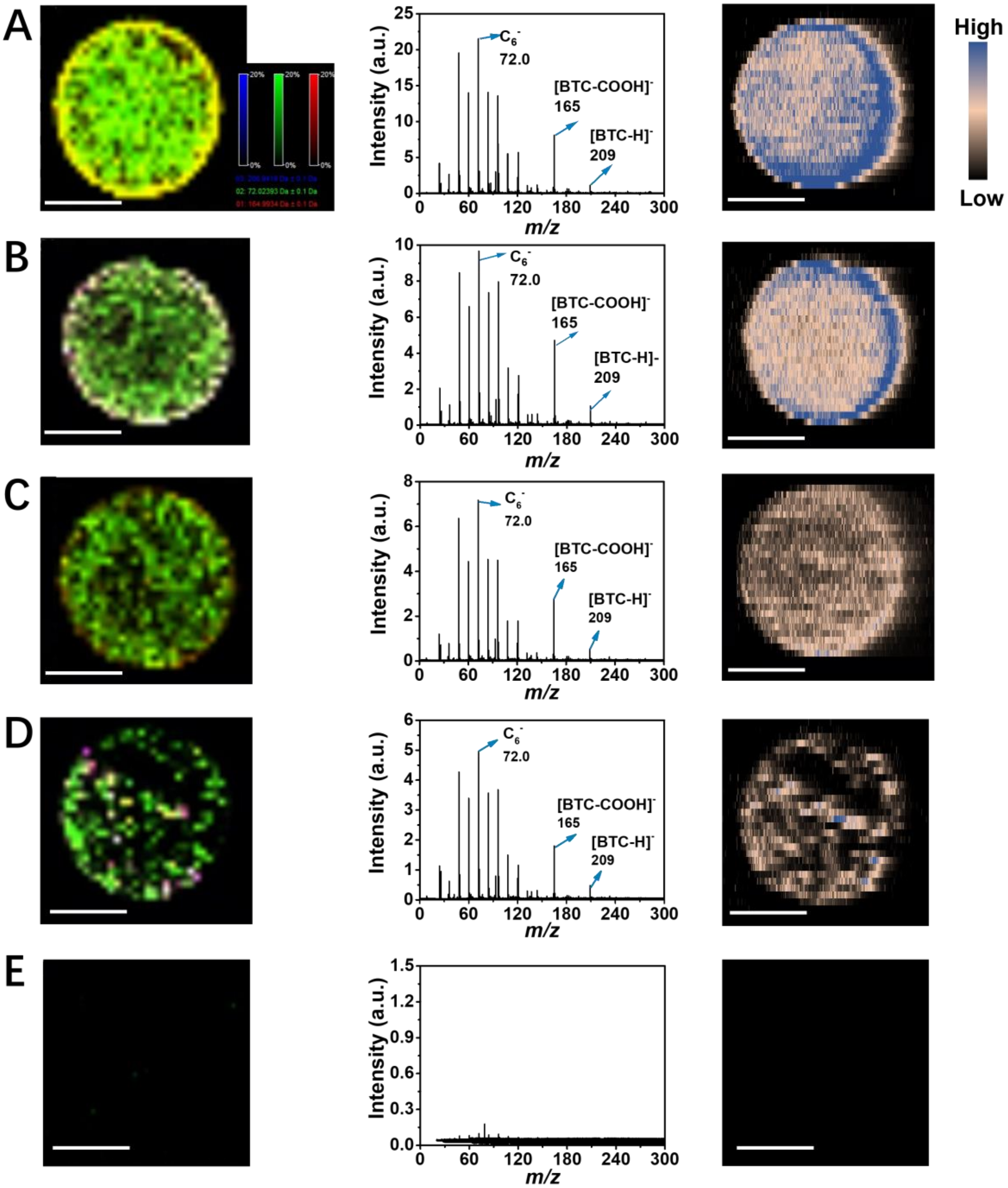

Figure S3. Characterization of CuBTC at **(A)** 0.8 mg/mL, **(B)** 0.4 mg/mL, **(C)** 0.1 mg/mL, **(D)** 0.05 mg/mL, and **(E)** 0 mg/mL. For each concentration, the left column is LDI-SRMS imaging result and the original image color of each ion is generated by the primary colors red (*m/z* 165), green (*m/z* 72.0) and blue (*m/z* 209). The middle column is the corresponding LDI-SRMS spectra, and the right column is LA-ICP-MS imaging result. The spatial resolution of imaging is 50 μm and the scale bar is 1 mm.

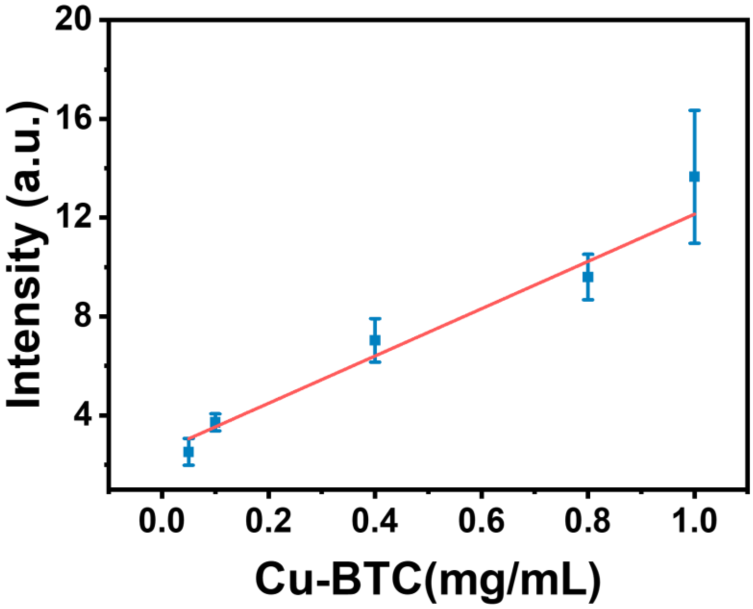

Figure S4. The linear relationship between the peak intensity of LDI-SRMS signal (*m/z* 165) and the CuBTC concentration.

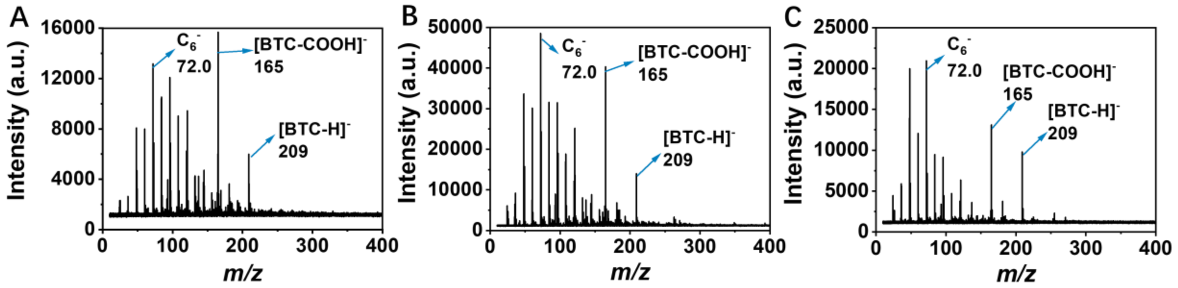

Figure S5. Typical LDI-SRMS spectra of **(A)** newly synthetic CuBTC (CuBTC-1) dispersed in ethanol, **(B)** aged CuBTC (two months after synthesis, CuBTC-2) dispersed in ethanol, and **(C)** newly synthetic CuBTC-1 dispersed in distilled water.

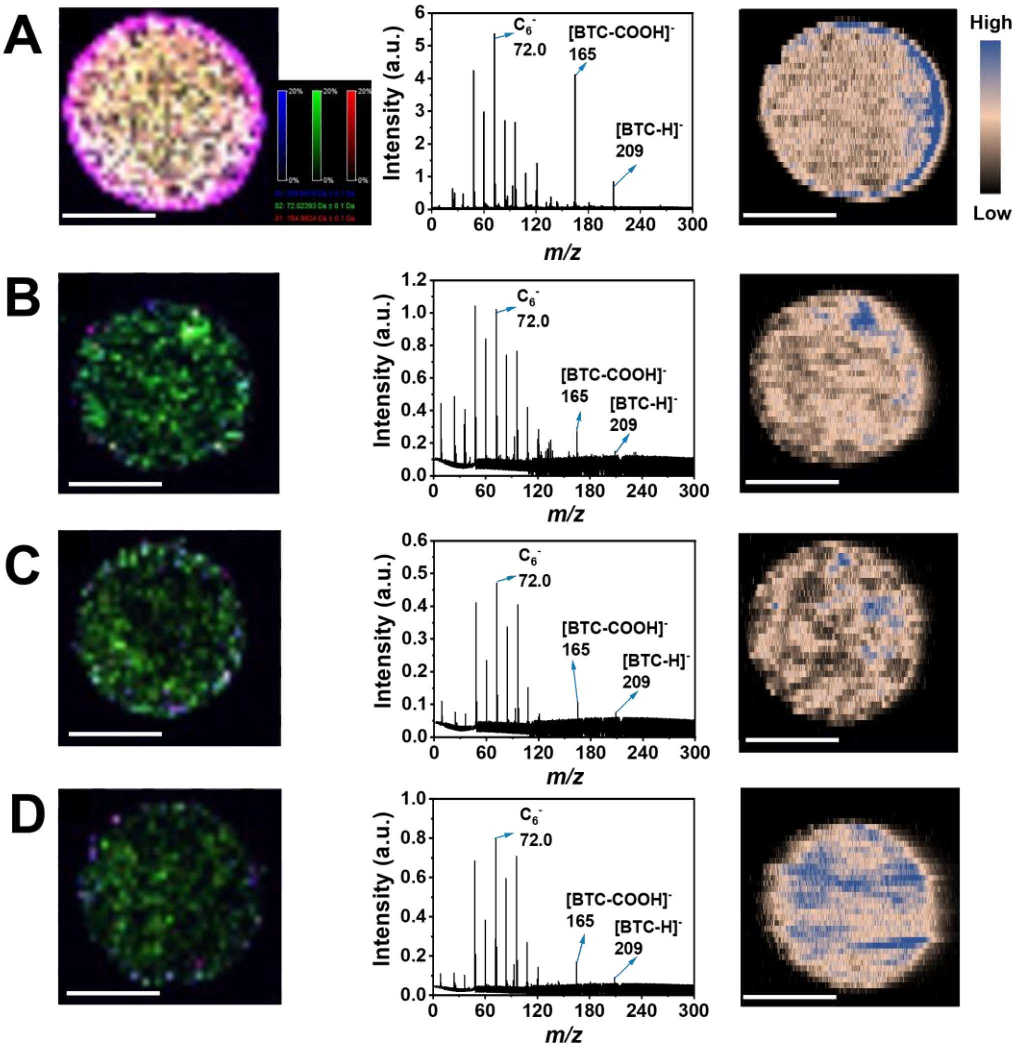

Figure S6. MS characterization of CuBTC in water for different periods of time. Standing time: **(A)** 15 min, **(B)** 60 min, **(C)** 150 min and **(D)** 240 min. For each standing time, the left column is LDI-SRMS imaging result and the original image color of each ion is generated by the primary colors red (*m/z* 165), green (*m/z* 72.0) and blue (*m/z* 209). The middle column is the corresponding LDI-SRMS, and the right column is LA-ICP-MS imaging result. The spatial resolution of imaging is 50 μm and the scale bar is 1 mm. The slight difference in the Cu^{2+} concentration showed no time-dependence and should be caused by the concentration variation of CuBTC dispersion due to its poor solubility.

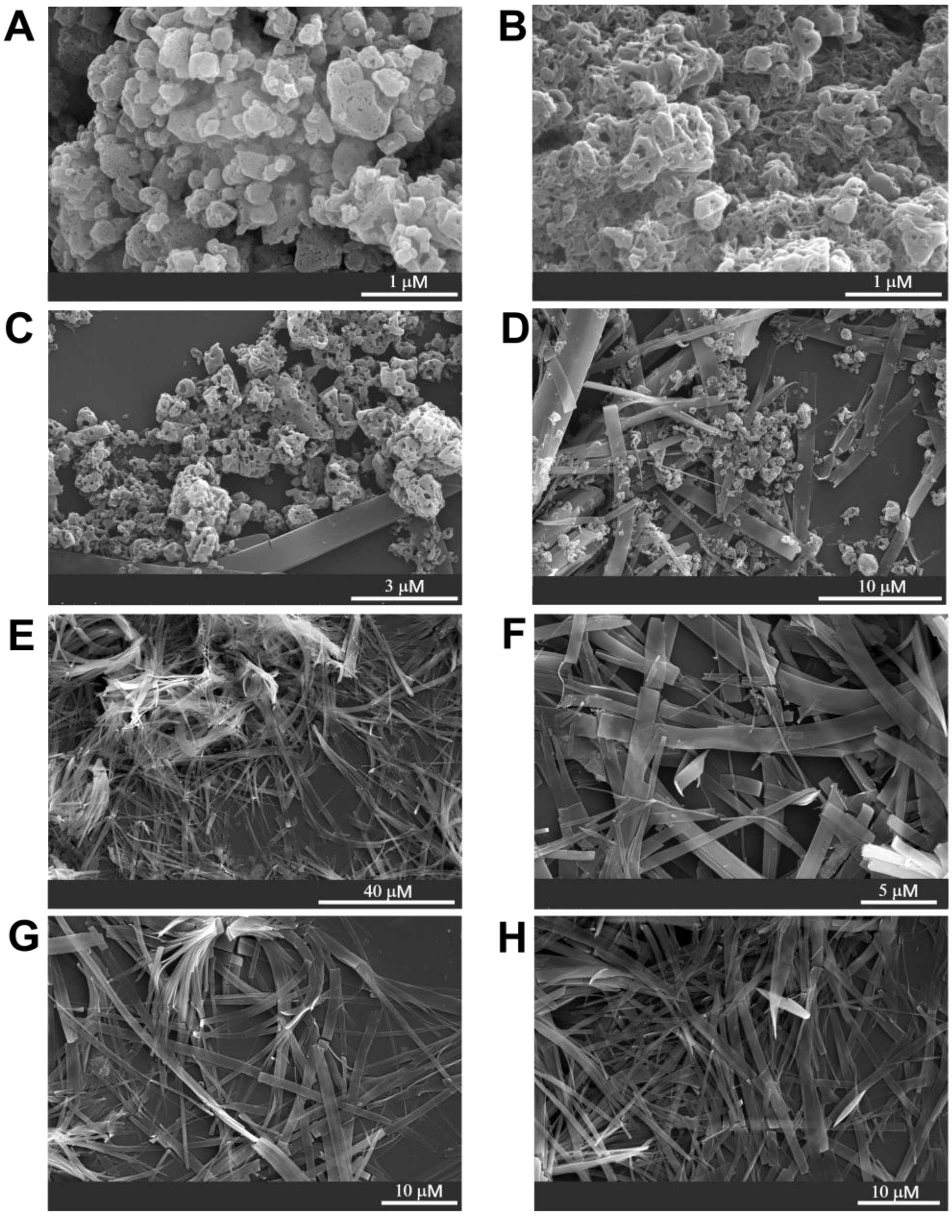

Figure S7. SEM characterization of CuBTC after dispersion in water for different periods of time. Standing time: **(A)** 5 min, **(B)** 15 min, **(C)** 40 min, **(D)** 60 min, **(E)** 120 min, **(F)** 150 min, **(G)** 180 min, and **(H)** 240 min.

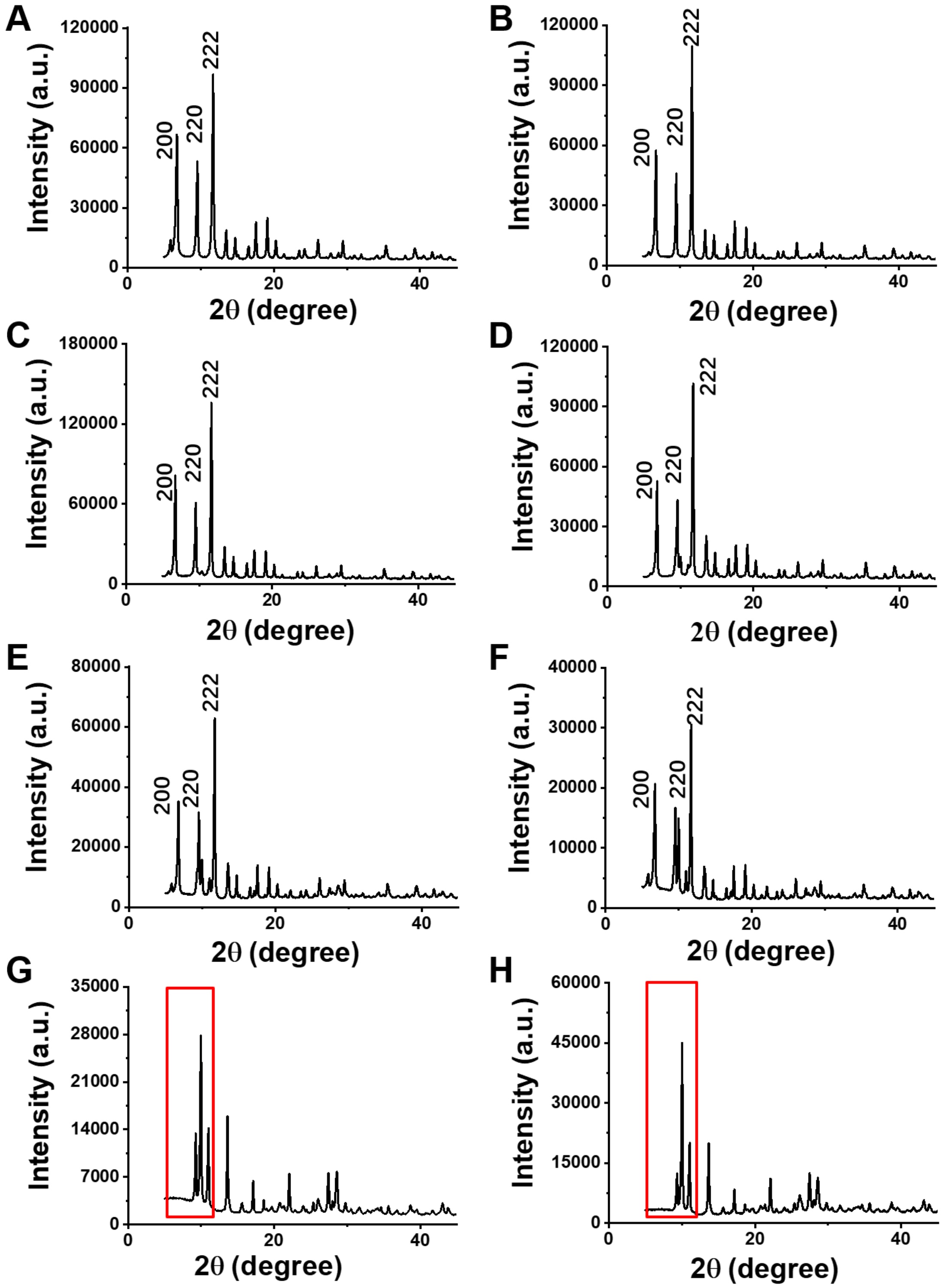

Figure S8. XRD patterns of CuBTC after dispersion in water for different periods of time. Standing time: **(A)** 5 min, **(B)** 15 min, **(C)** 40 min, **(D)** 60 min, **(E)** 120 min, **(F)** 150 min, **(G)** 180 min, and **(H)** 240 min. The peak intensity of [200] planes disappeared and [222] planes decreased sharply at 180 min (as shown in red frame).

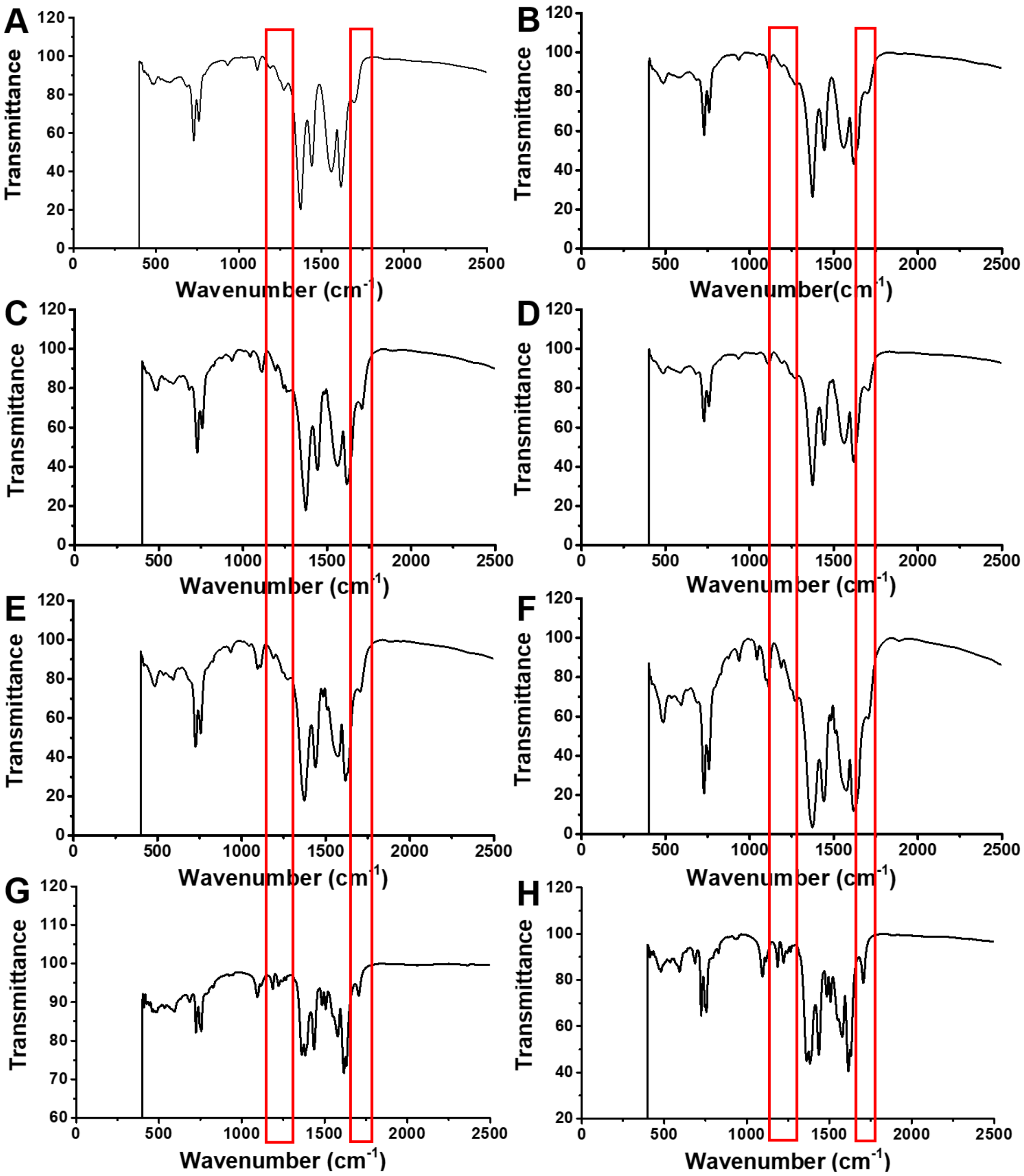

Figure S9. FTIR spectra of CuBTC after dispersion in water for different periods of time. Standing time: **(A)** 5 min, **(B)**15 min, **(C)** 40 min, **(D)** 60 min, **(E)** 120 min, **(F)** 150 min, **(G)** 180 min, and **(H)** 240 min. The characteristic bands of carboxylic acids at 1705 cm^{-1} for C=O stretching and bands at 1150–1280 cm^{-1} for C-O stretching were enhanced at 180 min of standing time, indicating the degradation of CuBTC and the presence of protonated carboxylate groups (as shown in red frame).

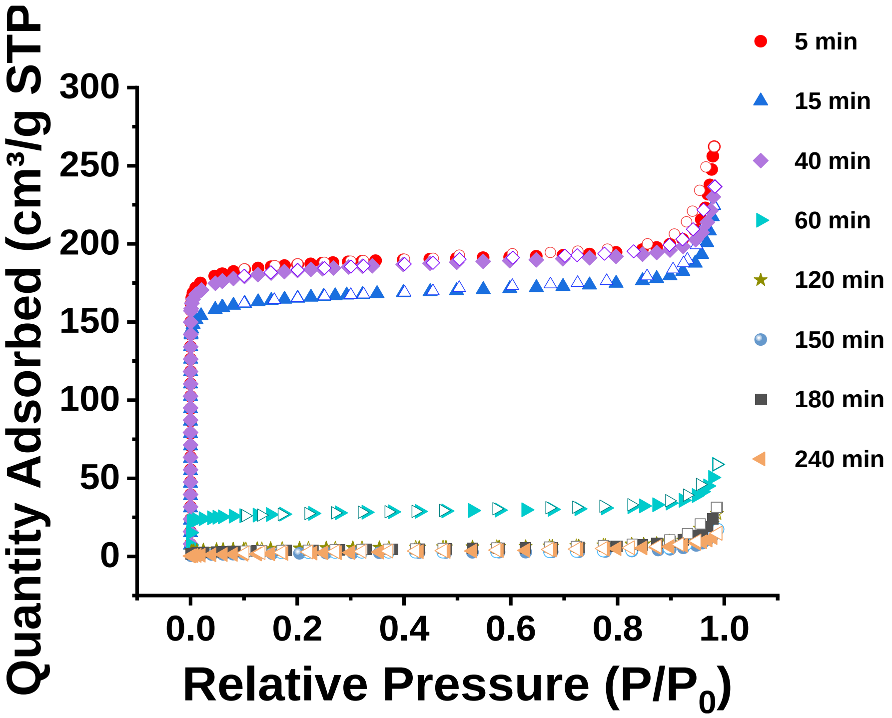

Figure S10. N_2 adsorption/desorption isotherms of CuBTC after dispersion in water for different periods of time. Standing time: **(A)** 5 min, **(B)** 15 min, **(C)** 40 min, **(D)** 60 min, **(E)** 120 min, **(F)** 150 min, **(G)** 180 min, and **(H)** 240 min.

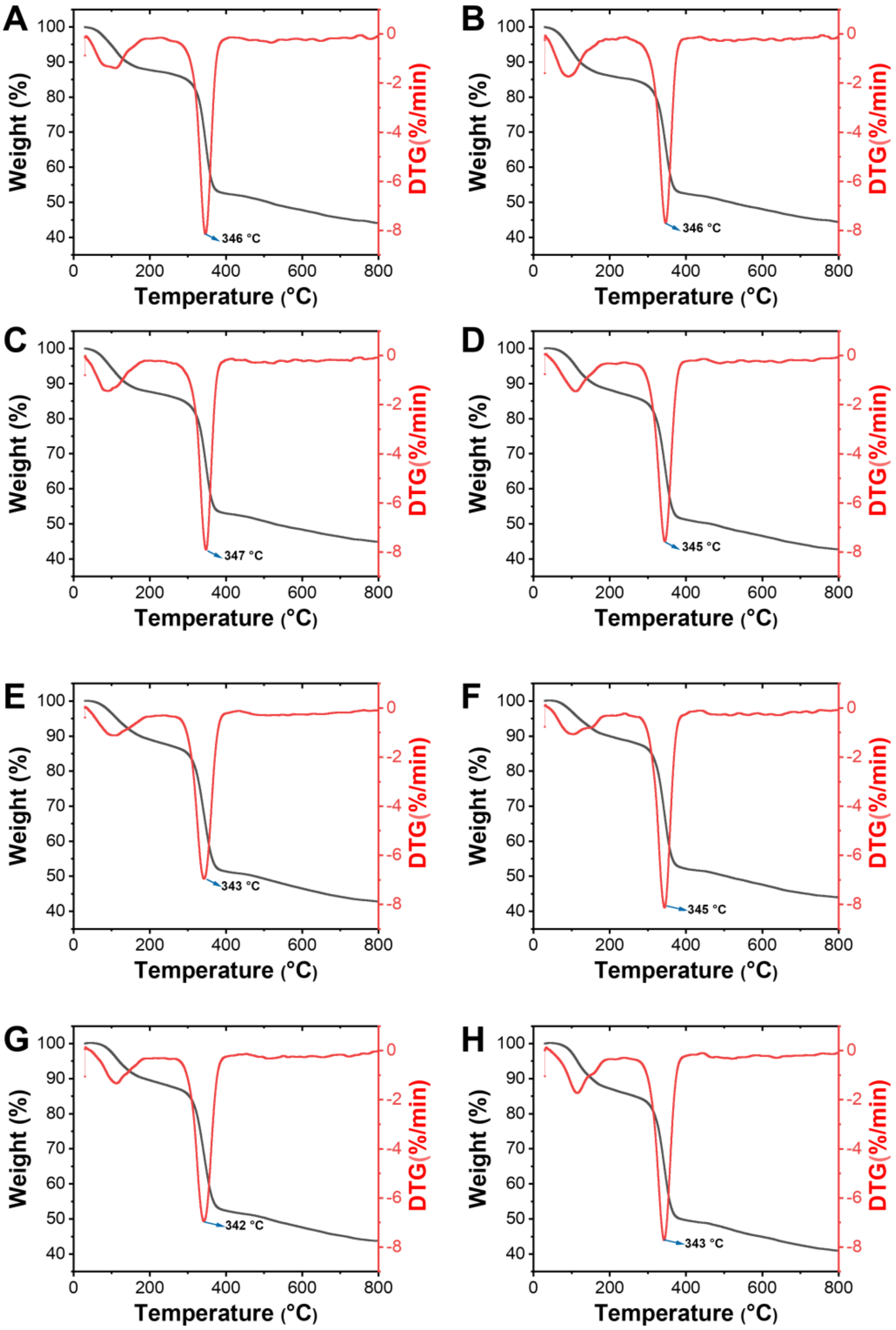

Figure S11. Thermogravimetry analysis of CuBTC after dispersion in water for different periods of time. Standing time: **(A)** 5 min, **(B)**15 min, **(C)** 40 min, **(D)** 60 min, **(E)** 120 min, **(F)** 150 min, **(G)** 180 min, and **(H)** 240 min.

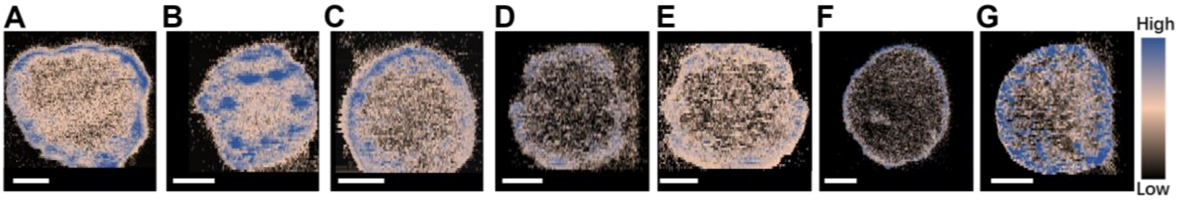

Figure S12. LA-ICP-MS imaging of CuBTC based on Cu signal after exposed to air for different periods of time. Exposure time: **(A)** 10 min, **(B)** 30 min, **(C)** 24 h, **(D)** 168 h, **(E)** 336 h, **(F)** 504 h, and **(G)** 720 h. The spatial resolution of LA-ICP-MS imaging is 50 μm and the scale bar is 1 mm.

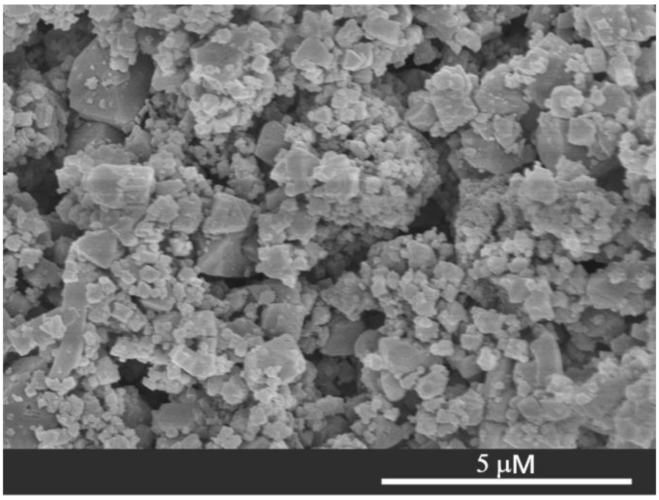

Figure S13. High-resolution SEM picture of CuBTC with a high concentration area in Figure 3C.

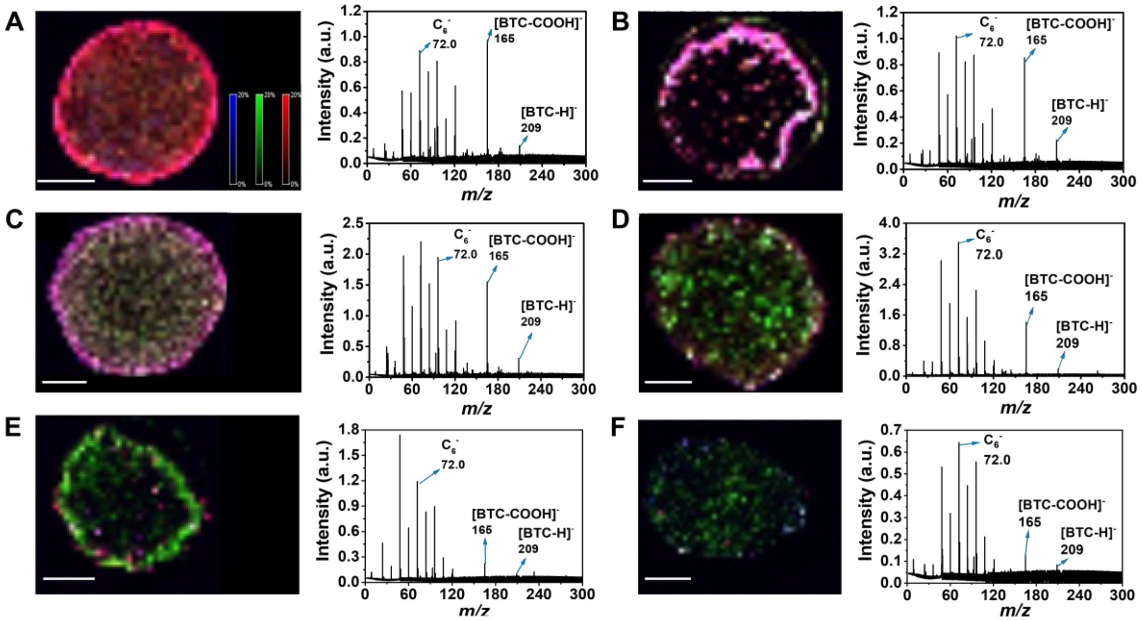

Figure S14. Characterization of CuBTC after exposed to CO_2 for different periods of time. Exposure time: **(A)** 30 min, **(B)** 1 h, **(C)** 72 h, **(D)** 336 h, **(E)** 720 h, and **(F)** 840 h. For each exposure time, the left column is LDI-SRMS imaging results and the original image color of each ion is generated by the primary colors red (*m/z* 165), green (*m/z* 72.0) and blue (*m/z* 209). The right column is the corresponding LDI-SRMS of CuBTC. The spatial resolution of LDI imaging is 50 μm and the scale bar is 500 μm. The peak intensity ratio of [BTC-COOH]$^-$ and [BTC-H]$^-$ (C_6^- as reference) was decreased as the exposure time increasing, indicating the degradation of CuBTC in CO_2.

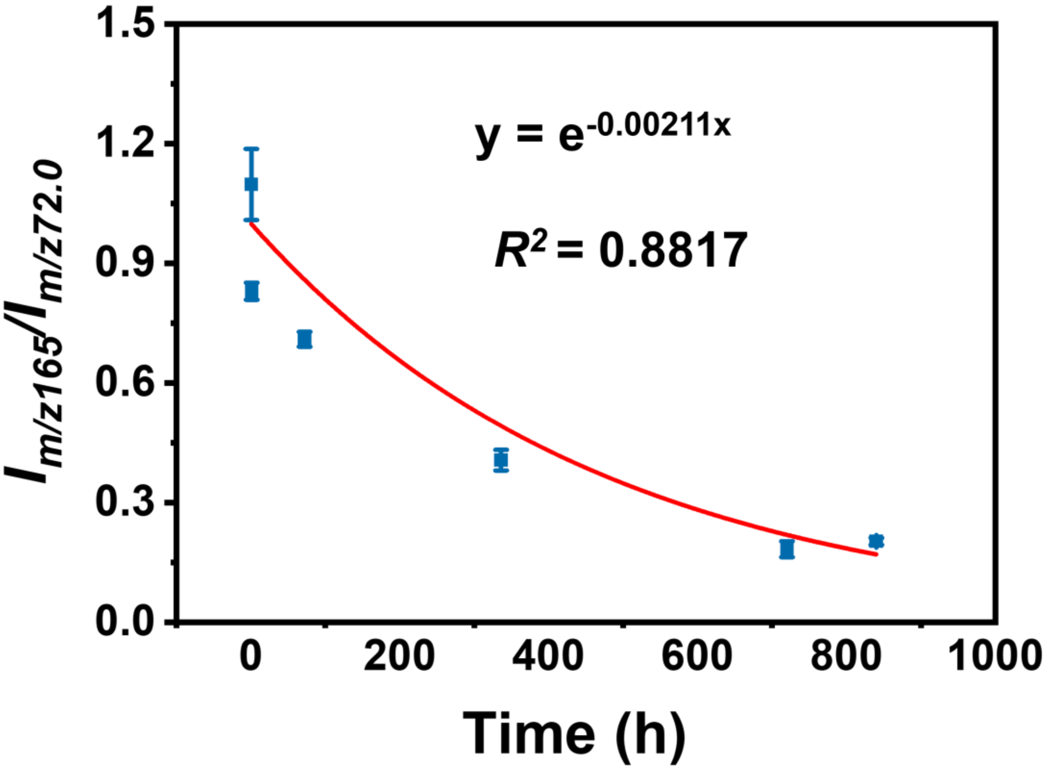

Figure S15. The relationship between $I_{m/z\ 165}/I_{m/z\ 72.0}$ and exposure time in CO_2. Exposure time: 30 min, 1 h, 72 h, 336 h, 720 h and 840 h.

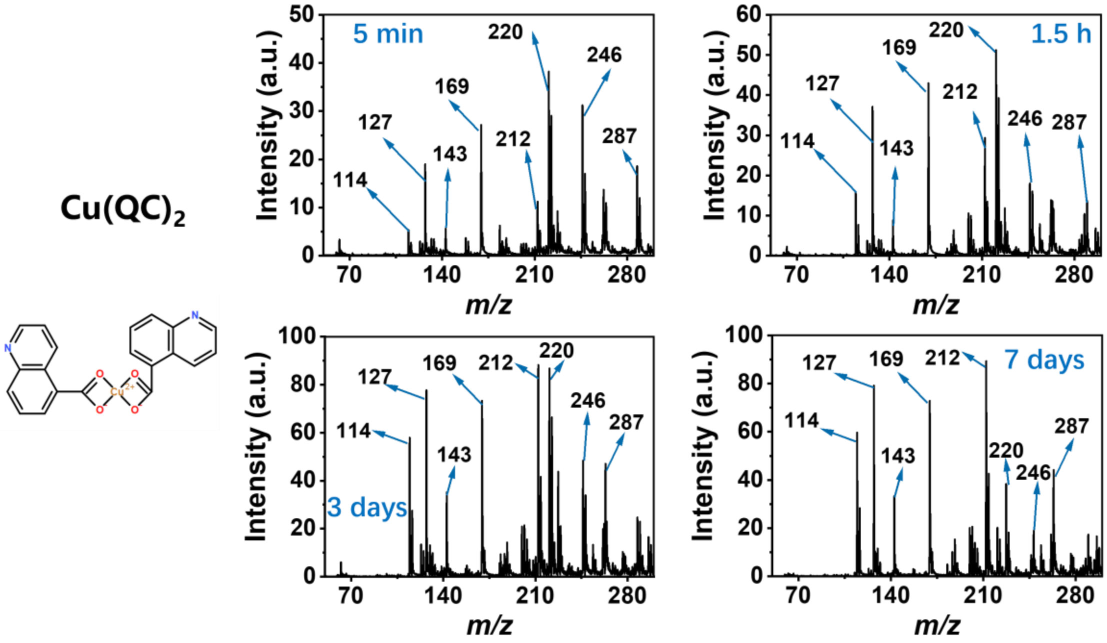

Figure S16. LDI-SRMS results of Cu(QC)$_2$ at *m/z* 50 to 300 in water for different periods of time (Standing time: 5 min, 1.5 h, 3 days and 7 days).

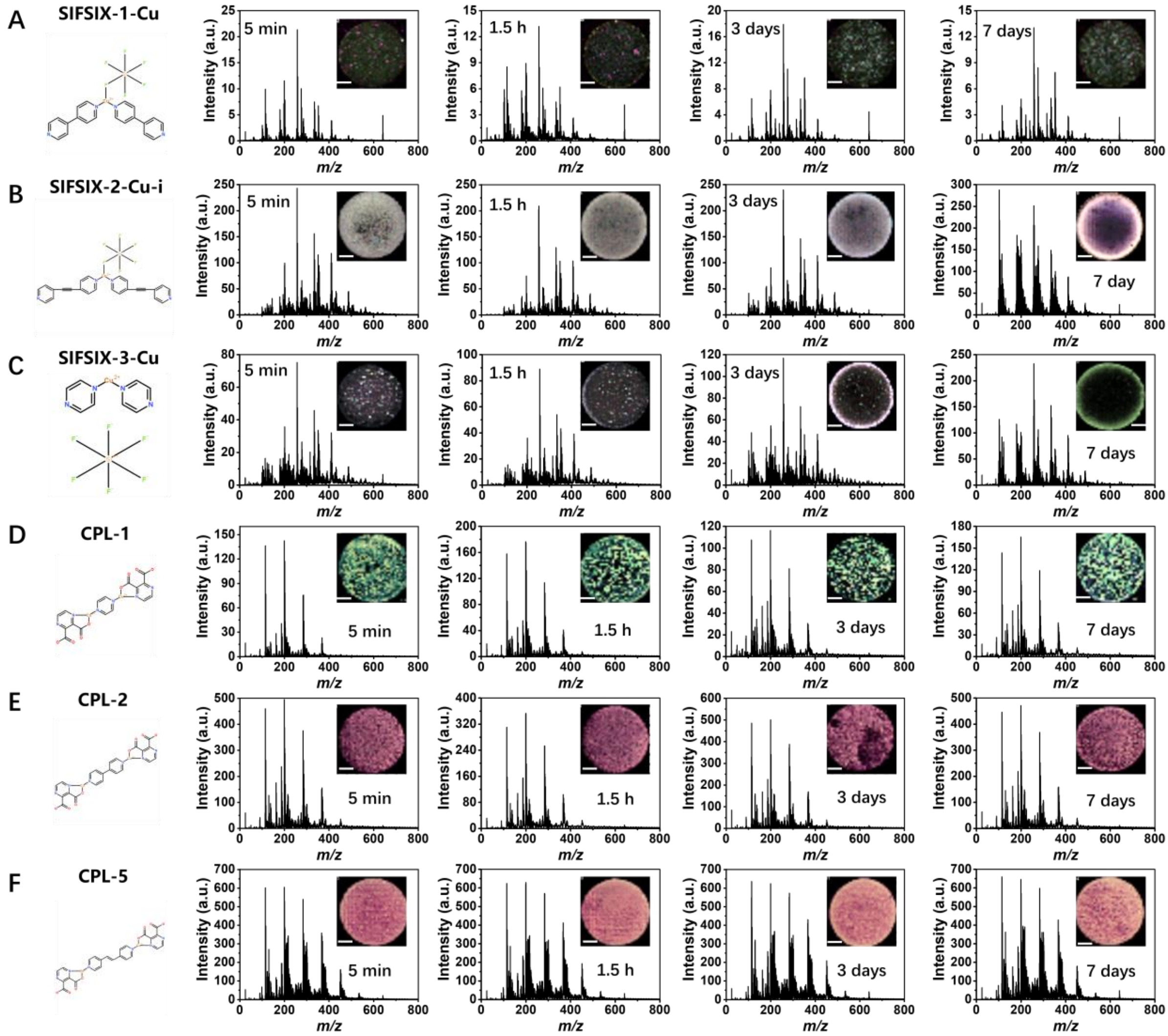

Figure S17. Characterization of Cu-MOFs in water for different periods of time. Standing time: 5 min, 1.5 h, 3 days and 7 days. LDI-SRMS and imaging results for **(A)** SIFSIX-1-Cu, **(B)** SIFSIX-2-Cu-i, **(C)** SIFSIX-3-Cu, **(D)** CPL-1, **(E)** CPL-2, and **(F)** CPL-5. The spatial resolution of LDI imaging is 50 μm and the scale bar is 500 μm. Characteristics peaks: *m/z* 102, 123, 181, 114, 201, 257, 275 and 334 for SIFSIX-1-Cu, *m/z* 114, 179, 201, 220, 238, 257, 275, 285, 334 and 412 for SIFSIX-2-Cu-I, 114, 137, 163, 187, 200 and 369 for SIFSIX-3-Cu, *m/z* 102, 145, 157, 279, 315, 334, 351, 431 and 488 for CPL-1, *m/z* 114, 130, 137, 163, 187, 200 and 367 for CPL-2, *m/z* 114, 130, 137, 163, 187, 200 and 367 for CPL-5 were chosen for SRMS imaging.

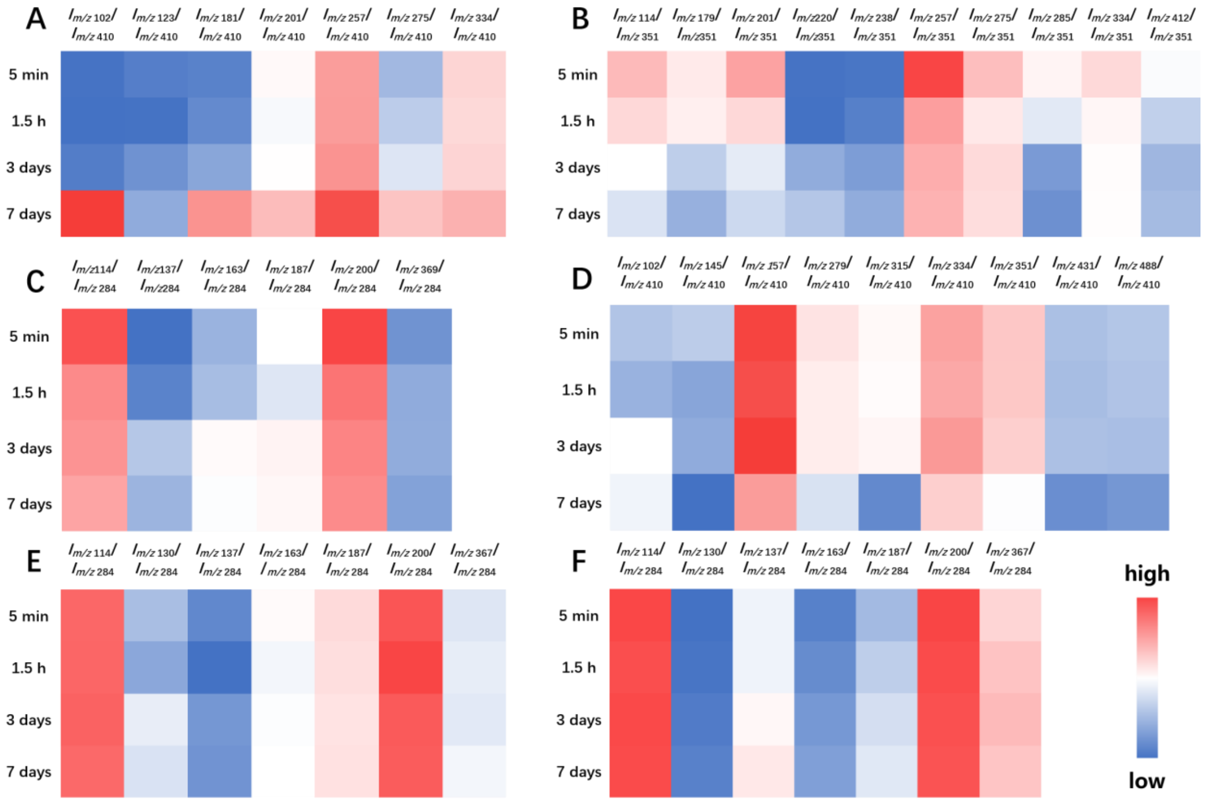

Figure S18. Heat map of intensity ratios for characteristic peaks of Cu-MOFs in water for different periods of time. Standing time: 5 min, 1.5 h, 3 days and 7 days**.** **(A)** SIFSIX-1-Cu, **(B)** SIFSIX-2-Cu-i, **(C)** SIFSIX-3-Cu, **(D)** CPL-1, **(E)** CPL-2, and **(F)** CPL-5. The peaks at *m/z* 410 of SIFSIX-1-Cu, *m/z* 351 of SIFSIX-2-Cu-i, *m/z* 284 of SIFSIX-3-Cu, *m/z* 410 of CPL-1, *m/z* 284 of CPL-2, *m/z* 284 of CPL-5 were chosen as reference for calculating ratios.

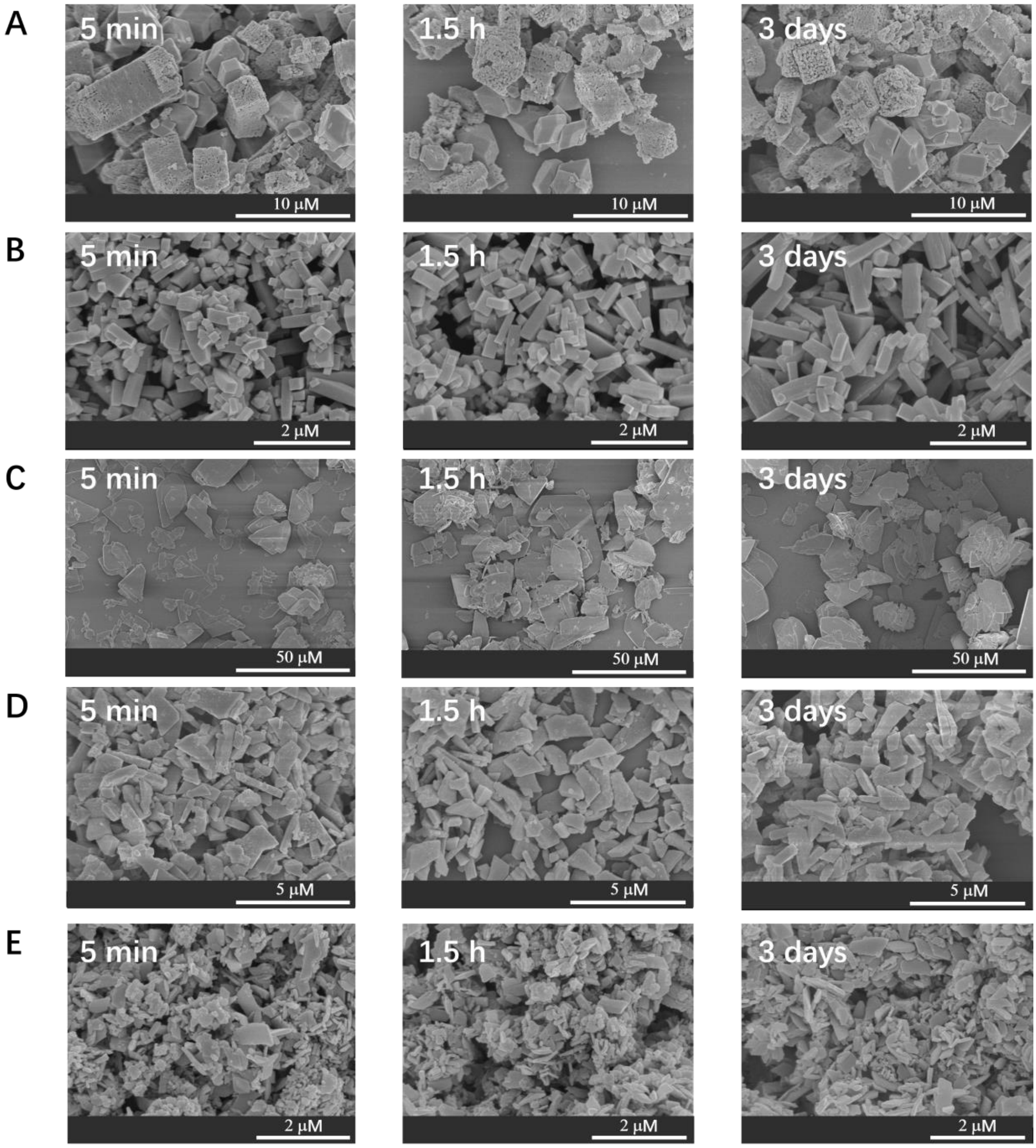

Figure S19. Typical SEM pictures of Cu-MOFs in water for different periods of time. Standing time: 5 min, 1.5 h, and 3 days. **(A)** SIFSIX-1-Cu, **(B)** SIFSIX-2-Cu-i, **(C)** CPL-1, **(D)** CPL-2, and (E) CPL-5.

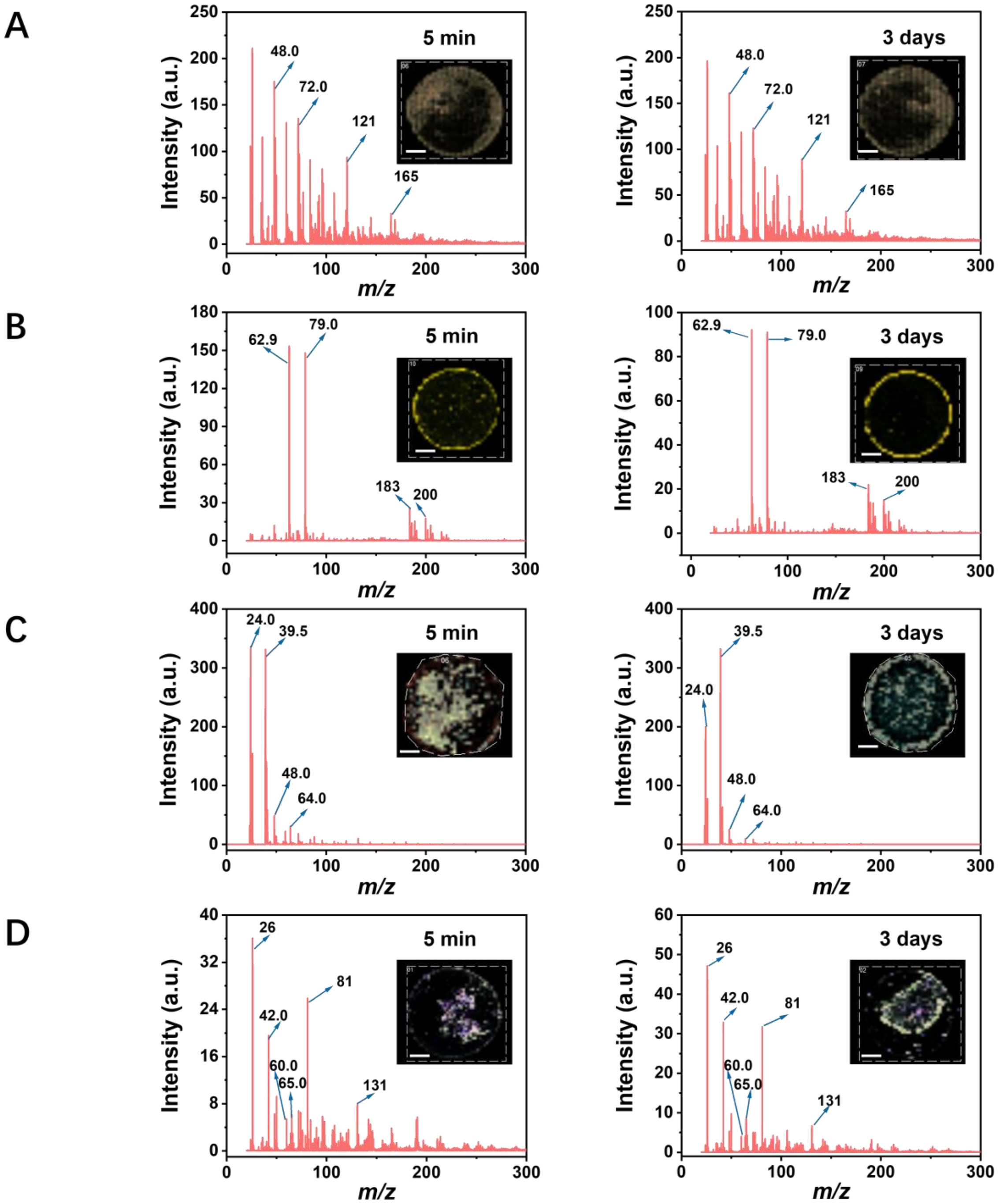

Figure S20. Characterization of non-copper MOFs in water for 5 min and 3 days. LDI-SRMS and imaging results for **(A)** MIL-101 (Cr), **(B)** Ni-containing MOF, **(C)** MOF-74 (Zn) and **(D)** ZIF-8 (Zn). The spatial resolution of LDI imaging is 50 μm and the scale bar is 500 μm.

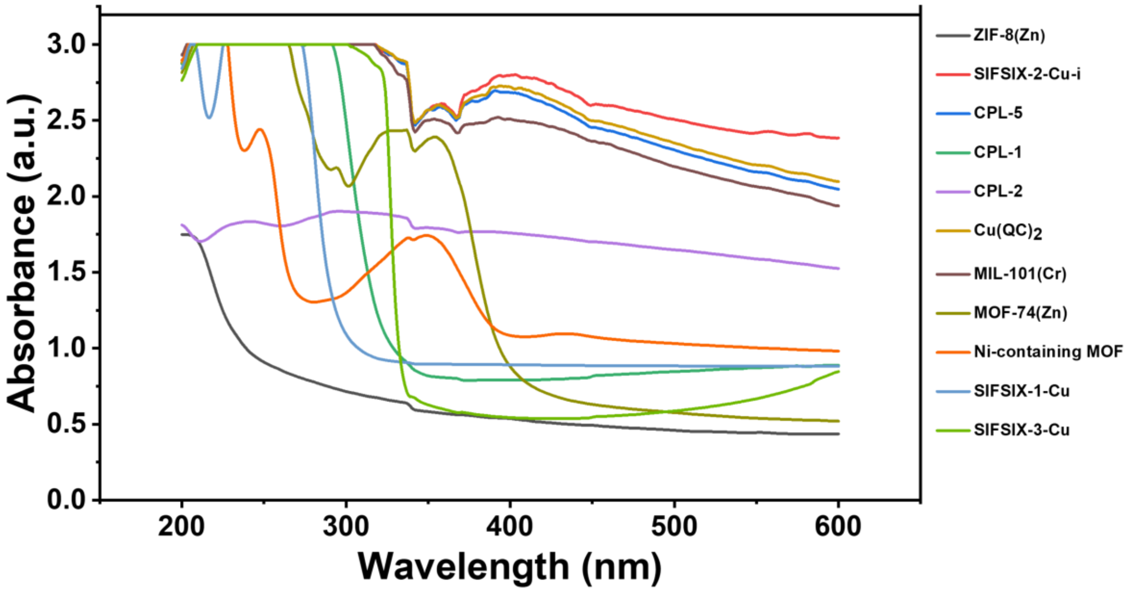

Figure S21. UV-Vis spectra of eleven common MOFs.

4. Supporting Tables

Table S1. Coefficient of variation for $I_{m/z\ 165}/I_{m/z\ 72}$ at different standing time in water.

standing time (min)	coefficient of variation for $I_{m/z\ 165}/I_{m/z\ 72}$
5	0.0380
15	0.0521
40	0.0465
60	0.0667
120	0.0500
150	0.0714
180	0.0842
240	0.0952

Table S2. Porosity data of CuBTC after dispersion in water for different periods of time.

Time (min)	BET Surface Area (m^2/g)	Pore volume (cm^3/g)	Pore Size (nm)
5	751	0.406	2.16
15	660	0.347	2.11
40	729	0.366	2.01
60	104	0.0910	3.50
120	17.9	0.0423	9.47
150	7.42	0.0268	14.5
180	14.1	0.0485	13.7
240	9.42	0.0229	9.72

Table S3. Coefficient of variation for $I_{m/z\ 165}/I_{m/z\ 72}$ at different standing time in air.

standing time (min)	coefficient of variation for $I_{m/z\ 165}/I_{m/z\ 72}$
0.167	0.0486
0.5	0.0712
24	0.0374
168	0.0647
336	0.0710
504	0.1190
720	0.1090

Table S4. Coefficient of variation for $I_{m/z\ 165}/I_{m/z\ 72}$ at different standing time in CO_2.

standing time (min)	coefficient of variation for $I_{m/z\ 165}/I_{m/z\ 72}$
0.5	0.0811
1	0.0258
72	0.0266
336	0.0634
720	0.1090
840	0.0429

Table S5. Change trends of intensity ratio of characteristic peaks for Cu-MOFs with the exposure time prolonging in water.

MOFs type	Organic ligands	$I_{(m/z)x}/I_{(m/z)y}$ changes as MOFs degradation
Cu(QC)$_2$	Quinoline-5-carboxylic acid	$I_{m/z\ 114}/I_{m/z\ 169}\uparrow$, $I_{m/z\ 127}/I_{m/z\ 169}\uparrow$, $I_{m/z\ 143}/I_{m/z\ 169}\uparrow$, $I_{m/z\ 212}/I_{m/z\ 169}\uparrow$, $I_{m/z\ 220}/I_{m/z\ 169}\downarrow$, $I_{m/z\ 246}/I_{m/z\ 169}\downarrow$, $I_{m/z\ 287}/I_{m/z\ 169}\downarrow$
SIFSIX-2-Cu-i	1,2-bis(4-pyridyl)ethyne	$I_{m/z\ 102}/I_{m/z\ 410}\uparrow$, $I_{m/z\ 123}/I_{m/z\ 410}\uparrow$, $I_{m/z\ 181}/I_{m/z\ 410}\uparrow$, $I_{m/z\ 201}/I_{m/z\ 410}\uparrow$, $I_{m/z\ 257}/I_{m/z\ 410}\uparrow$, $I_{m/z\ 275}/I_{m/z\ 410}\uparrow$, $I_{m/z\ 334}/I_{m/z\ 410}\uparrow$
SIFSIX-3-Cu	1,2-bis(4-pyridyl)ethyne	$I_{m/z\ 102}/I_{m/z\ 410}\uparrow$, $I_{m/z\ 145}/I_{m/z\ 410}\downarrow$, $I_{m/z\ 257}/I_{m/z\ 410}\downarrow$, $I_{m/z\ 279}/I_{m/z\ 410}\downarrow$, $I_{m/z\ 315}/I_{m/z\ 410}\downarrow$, $I_{m/z\ 334}/I_{m/z\ 410}\downarrow$, $I_{m/z\ 351}/I_{m/z\ 410}\downarrow$, $I_{m/z\ 431}/I_{m/z\ 410}\downarrow$, $I_{m/z\ 488}/I_{m/z\ 410}\downarrow$
SIFSIX-1-Cu	1,2-bis(4-pyridyl)ethyne	$I_{m/z\ 114}/I_{m/z\ 351}\downarrow$, $I_{m/z\ 179}/I_{m/z\ 351}\downarrow$, $I_{m/z\ 201}/I_{m/z\ 351}\downarrow$, $I_{m/z\ 220}/I_{m/z\ 351}\uparrow$, $I_{m/z\ 238}/I_{m/z\ 351}\uparrow$, $I_{m/z\ 257}/I_{m/z\ 351}\downarrow$, $I_{m/z\ 275}/I_{m/z\ 351}\downarrow$, $I_{m/z\ 285}/I_{m/z\ 351}\downarrow$, $I_{m/z\ 334}/I_{m/z\ 351}\downarrow$, $I_{m/z\ 412}/I_{m/z\ 351}\downarrow$

*Intensity ratios of characteristic peaks for CPL-1, CPL-2, and CPL-5 showed nearly no change.

5. References for SI

[1] N. Aljanabi, A. Alfutimie, F. R. Siperstein, X. L. Fan, *Front. Chem. Sci. Eng.* **2016**, *10,* 103-107.

[2] B. Levasseur, C. Petit, T. Bandosz, *ACS Appl. Mater. Interfaces*. **2010**, *2,* 3606-3613.

[3] S. H. Pang, C. Han, D. S. Sholl, C. W. Jones, R. P. Lively, *Chem. Mater.* **2016**, *28*, 6960-6967.

[4] D. O'Nolan, A. Kumar, M. J. Zaworotko, *J. Am. Chem. Soc.* **2017**, *139*, 8508-8513.